Noise Properties of Index-Guided Vertical-Cavity Surface-Emitting Lasers

Joanne Y. Law[1] and Govind P. Agrawal

The Institute of Optics and Rochester Theory Center
University of Rochester, Rochester, NY 14627

ABSTRACT

A numerical study of the noise characteristics of index-guided vertical-cavity surface-emitting lasers (VCSELs) is presented under single- and two-mode operation by considering the effects of spatial hole-burning and carrier diffusion on the intensity and frequency noise. In the case of single-mode operation, VCSEL noise properties are similar to those of edge-emitting lasers except for a diffusion-induced enhancement of the mode power. In the case of two-mode operation, VCSELs exhibit low-frequency enhancement of the intensity noise because of mode partition. The magnitude and the nature of the enhancement depend on the spatial profiles of the transverse modes supported by the VCSEL. By a proper design of the contact shape and size, it is possible to reduce the mode-partition noise in VCSELs.

Keywords: Surface-emitting lasers, transverse modes, laser noise, semiconductor device noise, diffusion processes

1. INTRODUCTION

Vertical-cavity surface-emitting lasers (VCSELs) have emerged in recent years as a new class of semiconductor lasers having several advantages associated with its unique cavity geometry. These advantages include low threshold current, single-longitudinal-mode operation, circular output beam, and wafer-scale integrability.[1,2] The performance of such lasers is improved considerably by using recently developed oxide-confined VCSELs[3–5] as index-guiding provided by the intracavity oxide aperture limits the number of transverse modes and stablizes their spatial profiles. Since VCSELs are attractive as compact light sources for applications in optical communications and interconnects, it is important to have a thorough understanding of their noise characteristics. Indeed, several experimental studies of the intensity noise in VCSELs have been performed.[6–10] However, theoretical modeling of VCSEL noise is often based on simple models which neglect spatial effects.[11–13] Since VCSELs have relatively large transverse dimensions, spatial effects are expected to be important, especially when a VCSEL operates in several transverse modes at high injection currents.[14] It has been found that VCSELs exhibit dynamic and static characteristics that are significantly different from those of edge-emitting lasers because of spatial hole-burning and carrier diffusion.[15–17] Such spatial effects are also expected to affect the VCSEL noise.

We have recently developed a numerical model of index-guided VCSELs that includes the spatial dependence of both the optical field and the carrier density and have used it to study the dynamical and noise aspects of VCSELs both with and without feedback.[18–23] In this paper, we present the results of this model for the noise properties of a VCSEL under both single-mode and two-mode operations. In particular, we consider several contact geometries capable of exciting different combinations of transverse modes. This approach allows us to investigate the role of intermodal coupling induced by spatial hole-burning. Our model, described in Section 2, includes the spatial dependence of both the optical field and the carrier density. Section 3 discusses the effect of carrier diffusion on the intensity, frequency, and phase noise under single-mode operation. In section 4 we study the noise characteristics under two-mode operation and investigates the effect of spatial hole-burning on mode-partition noise (MPN) through the use of two different

[1]Correspondence : jylaw@geocities.com

Part of the SPIE Conference on Physics and Simulation of Optoelectronic Devices VII
San Jose, California • January 1999 SPIE Vol. 3625 • 0277-786X/99/$10.00

contact geometries. Section 5 summarizes our main results. We do not consider in this paper the effects of optical feedback on noise and refer the reader to our previous work for a discussion of such effects[23] .

2. NUMERICAL MODEL

Assuming that the VCSEL can operate in M transverse modes simultaneously and making use of the cylindrical coordinates, the field and carrier-density equations for an index-guided VCSEL can be written as[18–23]

$$\frac{dE_i}{dt} = \frac{1}{2}(1 - j\alpha)[G_i(t) - \gamma_i]E_i + F_i(t), \qquad i = 1, 2, \ldots, M, \tag{1}$$

$$\frac{\partial N}{\partial t} = D\nabla_T^2 N + \frac{J(r,\phi)}{qd} - \frac{N}{\tau_e} - BN^2 - \frac{1}{d}\sum_{i=1}^{M} G_{local}|E_i(t)|^2|\psi_i(r,\phi)|^2, \tag{2}$$

where $E_i(t)$ is the amplitude of the i-th transverse mode with the spatial distribution $\psi_i(r,\phi)$, $N(r,\phi,t)$ is the carrier density, α is the linewidth enhancement factor, $G_i(t)$ and γ_i are the gain and cavity loss for the i-th mode. It is common to assume that all modes have the same loss γ. In Eq. (2), τ_e is the carrier lifetime due to nonradiative recombination, D is the diffusion coefficient, B is the spontaneous recombination coefficient, d is the thickness of the active layer, and $J(r,\phi)$ is the injection current density. In the small-signal regime, the local gain $G_{local} = a_0 v_g(N - N_T)/(1 + \epsilon_{NL}|E_i|^2)$ is assumed to be linearly proportional to the local carrier density $N(r,\phi,t)$, where N_T is the carrier density at transparency, a_0 is the gain cross-section, v_g is the group velocity, and ϵ_{NL} is the nonlinear-gain parameter.[24] Note that the field E_i is normalized such that $|E_i|^2$ corresponds to the photon number in the i-th mode.

The modal gain $G_i(t)$ for each mode in Eq. (1) is obtained by calculating the spatial overlap between the local-gain profile and the spatial intensity distribution $|\psi_i(r,\phi)|^2$ of that mode. It is given by

$$G_i(t) = \frac{\int_0^d\int_0^{2\pi}\int_0^{R_a} G_{local}(r,\phi,t)|\psi_i(r,\phi)|^2 \sin^2(\beta z) r\,dr\,d\phi\,dz}{\int_0^L\int_0^{2\pi}\int_0^{R} |\psi_i(r,\phi)|^2 \sin^2(\beta z) r\,dr\,d\phi\,dz}, \tag{3}$$

where R_a is the radius of the active region, R is the radius of the device, and L is the length of the VCSEL cavity. The propagation constant β is the same for all transverse modes since they are associated with the same longitudinal mode. Our model assumes that the local gain G_{local} is the same for all modes irrespective of their operating frequency. This assumption is justified since mode spacing ($\sim$ 100 GHz) is a small fraction of the gain bandwidth. The local gain depends on the mode intensity through the nonlinear-gain parameter ϵ_{NL}. However, the noise properties of VCSELs are not affected significantly by the nonlinear-gain reduction.

The effect of spontaneous emission is included by the Langevin noise term $F_i(t)$ in Eq. (1). It describes a Markoffian Gaussian random process with zero mean and δ-function correlation such that[24]

$$\langle F_i(t)\rangle = 0, \tag{4}$$

$$\langle F_i(t_1)F_j^*(t_2)\rangle = R_{sp}\delta_{ij}\delta(t_1 - t_2), \tag{5}$$

where $R_{sp} = n_{sp}\gamma$ is the average rate of spontaneous emissions into a laser mode, and n_{sp} is the spontaneous emission factor related to the degree of population inversion. For semiconductor lasers, an appropriate value of n_{sp} is about 2; we use $n_{sp} = 1.8$ in our numerical simulations.[24]

The average mode powers are obtained by solving Eqs. (1) and (2) with the $F_i(t)$ terms set to zero. In the presence of spontaneous emission, the laser output power fluctuates around this average value. The spectrum of such power

fluctuations is referred to as the intensity-noise spectrum. The intensity noise at a given frequency ω is characterized by the relative-intensity noise (RIN) defined as[24]

$$\text{RIN} = \frac{S_p(\omega)}{\bar{P}^2}, \tag{6}$$

where $\bar{P}$ is the average power. The spectral power density is given by

$$S_p(\omega) = \int_{-\infty}^{+\infty} \langle \delta P(t+\tau)\delta P(t)\rangle \exp(-j\omega\tau)d\tau, \tag{7}$$

where the angle brackets denote an ensemble average, and $\delta P(t)$ represents a small perturbation around the average power $\bar{P}$. The spectral power density $S_p(\omega)$ is related to the Fourier transform $\delta\tilde{P}(\omega)$ of $\delta P(t)$ by the simple relation:

$$S_p(\omega) = \langle |\delta\tilde{P}(\omega)|^2\rangle. \tag{8}$$

Since each spontaneously emitted photon changes the optical phase by a random amount, spontaneous emission not only produces the RIN in VCSELs but also leads to phase fluctuations that are responsible for frequency fluctuations and the linewidth of each laser mode in the optical spectrum. Phase fluctuations produce a frequency shift $\delta\omega = \delta\dot{\varphi}$, where $\dot{\varphi}$ denotes the time derivative of φ. The spectral density of the frequency noise, or the frequency-noise spectrum (FNS), is defined in a way similar to the RIN [see Eq. (7)] and is given by

$$S_{\dot{\varphi}}(\omega) = \int_{-\infty}^{+\infty} \langle \delta\dot{\varphi}(t+\tau)\delta\dot{\varphi}(t)\rangle \exp(-j\omega\tau)d\tau. \tag{9}$$

It can be related to the Fourier transform $\delta\tilde{\varphi}(\omega)$ of $\delta\varphi(t)$ by the simple relation

$$S_{\dot{\varphi}}(\omega) = \langle |\omega\delta\tilde{\varphi}(\omega)|^2\rangle. \tag{10}$$

The field and carrier equations [Eqs. (1) and (2)] are integrated numerically using a finite-difference method in both the temporal and spatial domains. The accuracy is maintained by choosing spatial and temporal resolutions fine enough that the numerical results do not change significantly with a decrease in step sizes. We use a temporal resolution of 0.1 ps and a spatial resolution of 0.1 μm along the radial direction. The intensity-noise and frequency-noise characteristics are calculated numerically by averaging over 30 trajectories, each of duration 26 ns, resulting in a resolution of 38 MHz over a 20-GHz frequency range.

The carrier-density equation requires an implicit solution in the radial direction due to the coupling introduced by the diffusion term. To solve for $N(r)$ at any given point in time, the spatial domain is divided evenly into 100 steps. The radial mesh runs from δr to $R = 10$ μm, where $\delta r = 0.1$ μm is the spatial resolution. The point $r = 0$ is excluded because of the singularity associated with the Laplacian term. The boundary conditions $N(0) = N(\delta r)$ and $N(R) = 0$ are used. Since the diffusion term involves a second-order derivative of $N(r)$, each $N(r)$ is coupled only to its nearest neighbors $N(r+\delta r)$ and $N(r-\delta r)$. Therefore, provided that the gain is a linear function of $N(r)$, the carrier equation can be casted into a tridiagonal matrix form, which can be easily inverted to obtain a solution for $N(r)$. In spite of the matrix-inversion involved, the computer code is reasonably fast. A typical run of a 26-ns trajectory takes less than 5 minutes on an Ultra-1 workstation.

For nunerical simulations we focus on an index-guided VCSEL with cylindrical geometry (index guiding over 4-μm radius). Our results are thus directly applicable to oxide-confined VCSELs that have been developed over the last few years.[3–5] We use realsitic device parameters as much as possible. Relevant device parameters used in the nunerical simulations are listed in Table 1. Transverse modes of an index-guided VCSEL are the LP_{mn} modes well-known in the context of optical fibers. However, one or more modes can be excited depending on the contact shape

Table 1: Device parameters used in numerical simulations

Cavity length L_{eff}	2 μm
Active-region thickness (3 QWs)	3×8 nm
Radius of device	10 μm
Radius of index-guiding region	4 μm
Diffusion constant D	30 cm^2/s
Nonradiative recombination time τ_e	5 ns
Bimolecular recombination coefficient B	1×10^{-10} cm^3/s
Refractive indices n_1, n_2	3.4, 3.5
Wavelength λ	0.875 μm
Gain cross-section a_0	2.0×10^{-16} cm^2
Group velocity v_g	8.8×10^9 cm/s
Carrier density at transparency N_T	2.2×10^{18} cm^{-3}
Linewidth enhancement factor α	3.0
Mirror reflectivities R_1, R_2	0.995
Internal loss α_{int}	20 cm^{-1}
Longitudinal confinement factor Γ_l	0.012

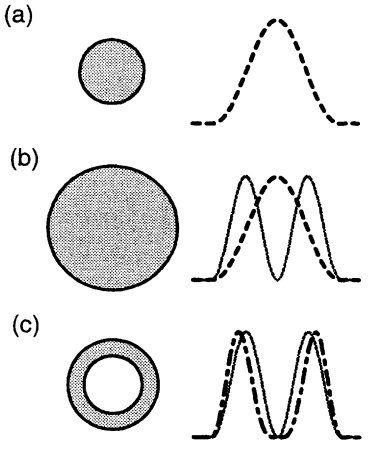

Figure 1. Three types of electrical contacts used and the corresponding intensity distributions of the transverse modes excited. (a) Narrow disc contact, (b) wide disc contact, and (c) ring contact. Dashed, solid and dot-dashed lines represent the LP_{01}, LP_{11}, and LP_{21} transverse modes, respectively. The horizontal scale for the mode profiles corresponds to a range of 10 μm.

and size and the injected current. The bias current is fixed at two times threshold throughout this study unless stated otherwise.

We first study how the shape and size of the electrical contact affect the transverse field distribution at a given current level by using three different contact geometries. The three types of electrical contacts used along with the radial intensity distributions of the transverse modes excited are shown in Fig. 1. Our numerical results show that single-mode operation (fundamental mode LP_{11}) can be realized by using a disc contact of 2-μm radius (see Fig. 1a)

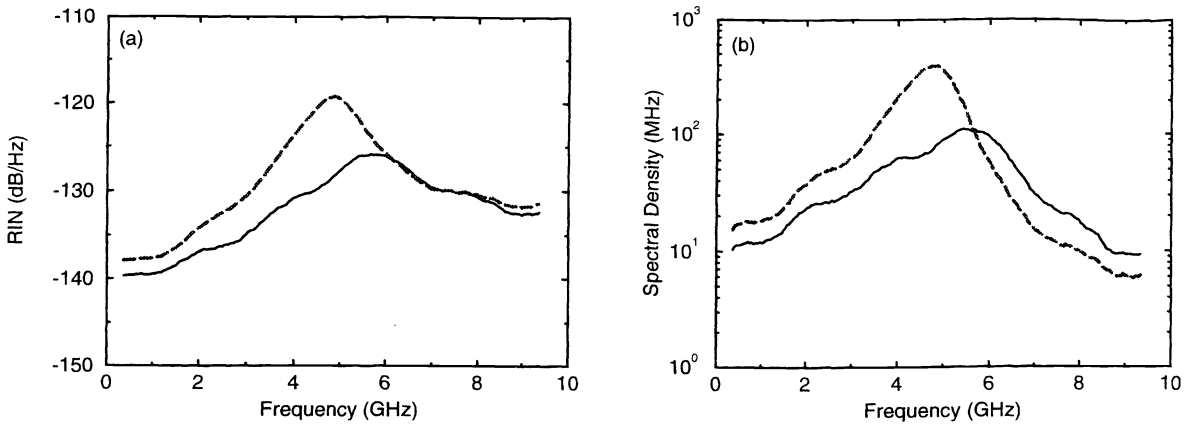

Figure 2. Noise characteristics under single-mode operation at two times above threshold. (a) RIN; (b) FNS. Solid and dashed traces correspond to diffusion constants of 30 and 1 cm^2/s, respectively.

such that current is injected only over a small central part of the VCSEL top area. For two-mode operation, different transverse modes can be excited by two different contact geometries. A 4-μm-radius disc contact (see Fig. 1b) excites the weakly overlapping LP_{01} and LP_{11} modes (weak-coupling case) while a ring contact (inner and outer radii of 1.8 and 2.8 μm, respectively) excites the strongly overlapping LP_{11} and LP_{21} modes as seen in Fig. 1c. (strong-coupling case). These two cases are referred to as the disc-contact and ring-contact geometries respectively in the following sections. A more detailed study of the effects of contact geometry on the lasing transverse-mode structures can be found in the literature[15] and.[25]

3. SINGLE-MODE OPERATION

We first consider the case in which the VCSEL operates in a single transverse mode (the LP_{01} mode) by using a narrow disc contact of 2-μm radius. The RIN spectrum at two times above threshold is shown as a solid line in Fig. 2a, corresponding to an output power of about 0.9 mW. The resonance peak near 6 GHz corresponds to the well-known relaxation-oscillation frequency.[24] The peak value of about -125 dB/Hz is of the same order of magnitude as that observed in edge-emitting lasers. The FNS shows a similar resonance peak near 6 GHz (solid line in Fig. 2b) because power fluctuations are related to fluctuations in the carrier population, which in turn lead to a phase change. The proportionality between the gain and index changes is provided by the linewidth enhancement factor α.

To investigate the effects of transverse carrier diffusion on noise characteristics, we have repeated the calculations for the case of negligible transverse diffusion by setting $D = 1$ cm^2/s. The RIN and FNS spectra are illustrated by the dashed lines in Figs. 2a and 2b, respectively. Transverse carrier diffusion is found to affect the RIN and FNS considerably. Our results show a 20-25% increase in the relaxation-oscillation frequency and a reduction by a factor of 5 in the peak height because of carrier diffusion, indicating its beneficial effects in VCSELs.

It is known that the linewidth of a single-mode semiconductor laser is related to the spectral density of the FNS at $\omega = 0$.[24] According to Fig. 2b, the linewidth of the VCSEL is about 16 MHz when diffusion effects are neglected (dashed line). With the inclusion of diffusion, the linewidth is reduced by about 50% and becomes 11 MHz. This result is surprising and somewhat counterintuitive. However, it can be understood easily if one considers the impact of spatial hole-burning on the radial distribution of the carrier density. Since diffusion fills the spatial hole at the mode center to some extent, the carrier density near the center of the circular contact where the mode intensity peaks is larger when the effects of carrier diffusion are included. Indeed, our calculations show that the output powers at two times above

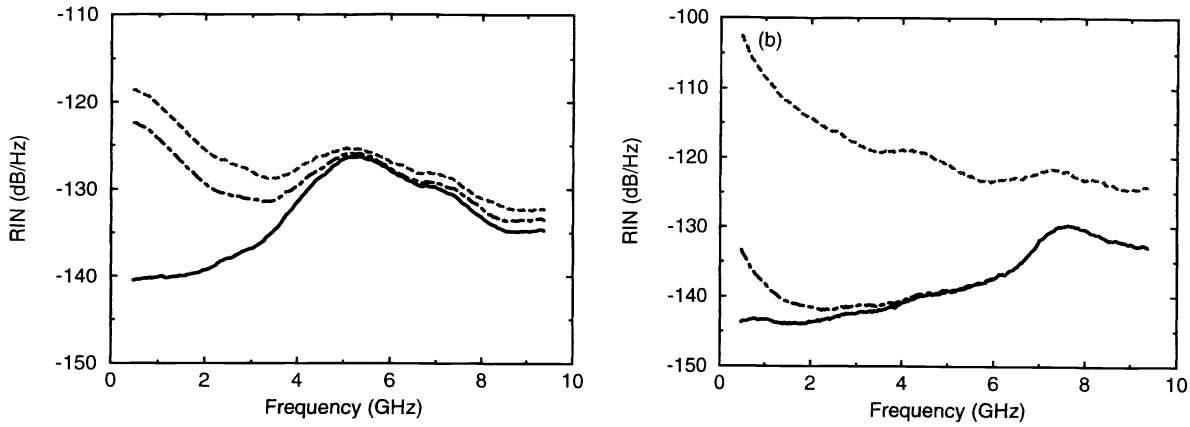

Figure 3. RIN characteristics under two-mode operation with a ring contact with injection current set at (a) 2 and (b) 3 times above threshold. Solid, dashed, and dot-dashed traces correspond to noise for the total power in both modes, the LP_{11} mode, and LP_{21} mode, respectively.

threshold are 0.9 mW and 0.6 mW respectively for $D = 30$ cm^2/s (significant diffusion) and 1 cm^2/s (negligible diffusion). Since the linewidth is inversely proportional to the output power,[24] the linewidth becomes narrower in the presence of diffusion because of a higher output power when the comparison is made at a constant current. These results shows that spatial effects such as spatial hole-burning and carrier diffusion are extremely important for understanding the noise properties of VCSELs under single-mode operation. Spatial effects become even more important when the VCSEL operates in several transverse modes simultaneously since various modes are coupled through the mechanism of gain saturation. We turn to the two-mode case in the next section.

4. TWO-MODE OPERATION

To investigate the effects of transverse-mode coupling, we consider two different contact geometries shown in Fig. 1. In the case of a 1.8-2.8 μm ring contact, VCSEL operates in LP_{11} and LP_{21} modes simultaneously. In contrast, in the case of a 4-μm disc contact the VCSEL operates in LP_{01} and LP_{11} modes. The main difference in the two cases is that two modes overlap significantly in the case of a ring contact whereas the mode overlap is minimum for a wide disc contact. It will be seen in this section that the noise properties of VCSELs are affected considerably by the degree of mode overlap.

The RIN spectra shown in Fig. 3a for the case of a ring contact correspond to 6-mA current (two times above threshold for the LP_{11} mode). The mode powers at this current level for the LP_{11} and LP_{21} modes are about 0.4 and 0.8 mW, respectively. Clearly, power fluctuations in individual transverse modes are larger by up to a factor of 100 (20-dB enhancement) than those of the total power for frequencies up to 4 GHz. This low-frequency-noise enhancement is known as mode-partition noise.[24] It arises when the two modes fluctuate in such a way as to leave the total power relatively constant due to the fact that the same carrier population provides gain for both modes. A random increase in the power of one mode induces a simultaneous decrease in the power of the other mode, which lasts a few nanoseconds because of relaxation oscillations. The LP_{11} mode exhibits larger fluctuations because of its lower average power. Mode-partition noise has been experimentally observed in both VCSELs and edge-emitting lasers.[8] In the case of VCSELs, transverse effects such as carrier diffusion and spatial hole-burning can affect the mode-partition noise dramatically, as will become clear from what follows.

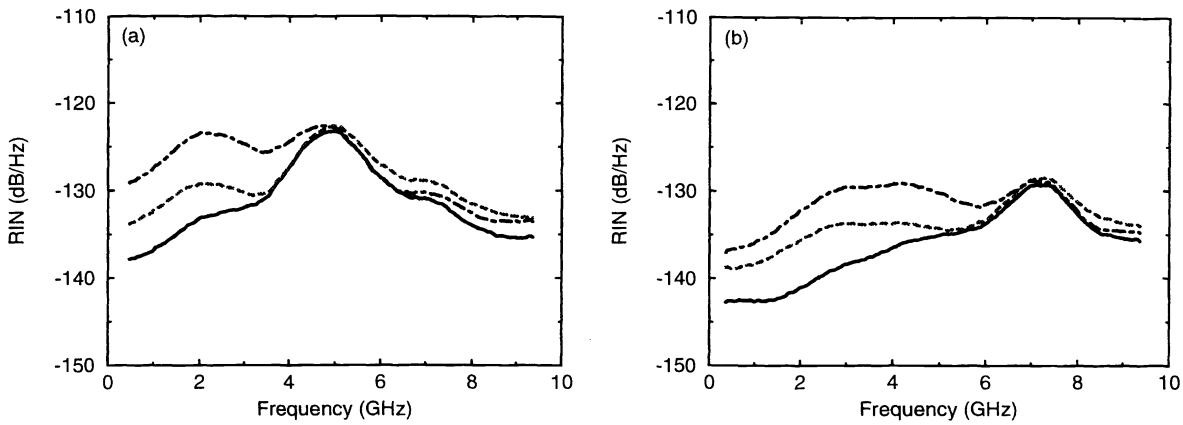

Figure 4. RIN characteristics under two-mode operation with a 4-μm-wide disc contact with injection current set at (a) 2 and (b) 3 times above threshold. Solid, dashed, and dot-dashed traces correspond to noise for the total power in both modes, the LP_{01} mode, and the LP_{11} mode, respectively.

Consider first the impact of the relative powers in each mode on the mode-partition noise. Since the spatial distributions of the LP_{11} and LP_{21} modes overlap significantly, as the current is increased, one mode becomes dominant while the other mode is suppressed due to carrier competition induced by spatial hole-burning.[15] Fig. 3b shows the RIN spectra under conditions identical to those of Fig. 3a except at three times above threshold, corresponding to powers of 0.1 and 2.3 mW in the LP_{11} and LP_{21} modes, respectively. The weak LP_{11} mode shows much higher RIN because of its lower average power, and the dominant LP_{21} mode exhibits RIN enhancement over a smaller frequency range (0–1 GHz). This behavior is reminiscent of that of edge-emitting lasers operating in a single spatial but several longitudinal modes. This is not surprising since longitudinal modes of an edge-emitting laser exhibit strong mode coupling thats also occurs for the ring-contact VCSEL because of a large spatial overlap between the mode profiles.

What happens to mode-partition noise when the VCSEL modes are weakly coupled? To investigate the effect of spatial hole-burning in this case, the RIN spectra for the case of a disc contact (4-μm radius) are shown in Fig. 4 under conditions identical to those of Fig. 3 except for different shape of the contact. In the case of a disc contact, VCSEL operates in the LP_{01} and LP_{11} modes, while the ring contact excites the LP_{11} and LP_{21} modes. The injected current through the VCSEL contact is two times above threshold for the LP_{01} mode, but the mode powers are nearly equal (about 0.7 mW) because of weak mode coupling resulting from a reduced mode overlap. The low-frequency enhancement of the RIN for individual modes is reduced by a factor of 10 compared with the case shown in Fig. 3a, even though the VCSEL operates in two modes in both cases. This result can be understood from the mode profiles shown in Fig. 1. The LP_{01} and LP_{11} modes have a smaller region of overlap, carrier competition is less intense for a disc contact, despite the fact that the two modes carry the same amount of power. At three times above threshold, mode-partition noise is found to be reduced so much that the low-frequency noise is lower than that occurring at the relaxation-oscillation peak in Fig. 4b. Thus, contrary to relatively high mode-partition noise seen in edge-emitting lasers operating in several longitudinal modes (but in a single transverse mode), multiple-transverse-mode VCSELs can be made with reduced mode-partition noise through the use of an appropriate pumping geometry.

An interesting feature of Fig. 4a is the appearance of a second peak near 2 GHz in addition to the relaxation-oscillation peak occurring at 5 GHz. Such a peak has never been observed in the RIN spectra of edge-emitting lasers, and its presence is solely due to multiple-transverse-mode operation. Its absence in Fig. 3 suggests that its origin lies in the disc-contact geometry. The LP_{01} and LP_{11} modes excited in such a VCSEL peak at $r = 0$ and $r \approx 2$ μm,

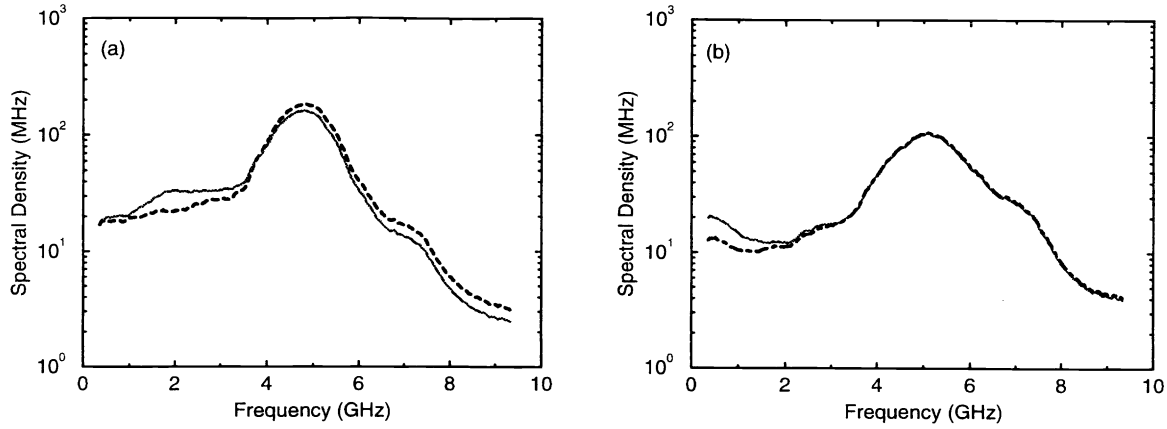

Figure 5. FNS under two-mode operation at 2 times above threshold with a (a) disc contact and (b) ring contact. Dashed, solid, and dot-dashed traces correspond to the LP_{01}, LP_{11}, and LP_{21} modes, respectively.

as seen in Fig. 1. In contrast, the ring-contact geometry excites the LP_{11} and LP_{21} modes, both of which peak near $r = 2\ \mu$m. A spatial hole is burnt in the carrier-density profile at the location where the mode intensity peaks. Clearly, two distinct spatial holes are burnt in the case of Fig. 4, whereas a single hole is burnt in the case of Fig. 3. As a result, carrier diffusion is much more effective in filling the spatial holes (and therefore reducing mode competition) in the case of a disc contact. For a diffusion constant of 30 cm^2/s and a carrier recombination time of about 2 ns, the effective diffusion rate is estimated to be in the range 2–3 GHz. Therefore, RIN enhancement is reduced due to diffusion effects for frequencies below 2 GHz but not in the frequency range 2–4 GHz, resulting in a shallow peak near 2 GHz. The inclusion of nonlinear gain reduces the peak values in Figs. 3 and 4 by about 2 dB, but the qualitative behavior remains unaffected.

The frequency-noise spectra at two times above threshold are shown in Figs. 5 for the two cases of disc and ring contacts, respectively. Due to the amplitude-phase coupling governed by the linewidth enhancement factor, the FNS show a relaxation-oscillation peak near 5 GHz similar to that observed in the RIN spectra in Figs. 3 and 4. However, the low-frequency enhancement of the frequency noise is much smaller than that occurring for the RIN spectrum. This can be understood by noting that gain saturation responsible for spatial hole burning depends on the mode intensities and is independent of the phases associated with the two transverse modes. In Fig. 5, the linewidths of individual modes (value of FNS for $\omega \to 0$) under two-mode operation are larger than the 11-MHz linewidth predicted for the single-mode case. This can be attributed to lower mode powers. Because of carrier sharing between the two modes, the power in each mode is reduced. This reduction of mode powers leads to an increase in linewidth. For two-mode operation with a disc contact (Fig. 5a), the linewidths of the two modes are nearly equal (about 17 MHz) since the two weakly coupled modes carry about the equal amount of power (0.7 mW). For two-mode operation with a ring contact (Fig. 5b), the linewidths of the LP_{11} and the LP_{21} modes are 20 MHz and 14 MHz, corresponding to output powers of 0.4 mW and 0.8 mW, respectively.

5. SUMMARY

In this paper we have investigated the effects of carrier diffusion and spatial hole-burning on the noise properties of index-guided VCSELs under both single-mode and two-mode operations. In the case of single-mode operation, carrier diffusion reduces the impact of spatial hole-burning by filling the spatial hole partially. This effect increases the mode

power, resulting in lower RIN and FNS. The relaxation-oscillation peak is not only damped but is also shifted to a higher frequency because of higher mode power. Higher mode power also results in a reduced linewidth.

In the case of two-mode operation, the low-frequency RIN for individual modes is found to be enhanced because of carrier competition induced by spatial hole-burning. This enhancement (mode-partition noise) also occurs for edge-emitting lasers. However, in the case of VCSELs, the nature of enhancement depends on the spatial profiles of the transverse modes. We have explored this effect by using two different contact geometries. For a ring contact, mode-partition noise is similar to that of edge-emitting lasers because of strong overlap of the mode profiles. In contrast, for a wide-disc contact, mode-partition noise is significantly reduced as a result of reduced carrier competition resulting from a smaller spatial overlap of the two transverse modes. The main conclusion is that the noise properties of index-guided VCSELs are quite sensitive to the design parameters, such as the shape and size of the electrical contact used for current injection, and thus can be controlled by a proper design. Our results are applicable to recently developed oxide-confined VCSELs and should be useful in understanding the performance of such devices.

ACKNOWLEDGMENTS

This work is partially supported by the National Science Foundation under Grant No. PHY94-15583.

REFERENCES

1. T.E. Sale, *Vertical-cavity Surface-emitting Lasers*, Wiley, New York, 1995.
2. C.J. Chang-Hasnain, in *Semiconductor Lasers: Past, Present and Future*, G.P. Agrawal, Ed., AIP Press, Woodbury, New York, 1995, Chap. 5.
3. H. Deng, Q. Deng, and D. G. Deppe, "Very small oxide-confined vertical-cavity surface-emitting lasers with a bulk active region," *Appl. Phys. Lett.*, **70**, 741–743 (1997).
4. B. Weigl, M. Grabherr, C. Jung, R. Jager, G. Reiner, R. Michalzik, D. Sowada, and K. J. Ebeling, "High-performance oxide-confined GaAs VCSELs," *IEEE J. Sel. Top. Quantum Electron.*, **3**, 409–415 (1997).
5. D. Sun and D. W. Treat, "Characteristics of native-oxide-confined InGaP-$(Al_xGa_{1-x})_{0.5}In_{0.5}P$ quantum-well ridge waveguide lasers," *IEEE Photon. Technol. Lett.* **10**, 492–494 (1998).
6. D.M. Kuchta, J. Gamelin, J.D. Walker, J. Lin, K.Y. Lau and J.S. Smith, "Relative Intensity Noise of Vertical Cavity Surface Emitting Lasers," *Appl. Phys. Lett.* **62**, 1194–1196 (1993).
7. K.H. Hahn, M.R. Tan, Y.M. Houng and S.Y. Wang, "Large area multitransverse-mode VCSELs for modal noise reduction in multimode fiber systems," *Electron. Lett.* **29**, 1482–1483 (1993).
8. M.S. Wu, L.A. Buckman, G.S. Li, K.Y. Lau and C.J. Chang-Hasnain, "Polarization induced enhancement of relative intensity noise and modulation distortion in vertical cavity surface emitting lasers," *14th IEEE Int. Semiconductor Laser Conf.*, pp. 145–146, IEEE, New York, 1994.
9. K.H. Hahn, M.R. Tan and S.Y. Wang, "Intensity noise of large area vertical cavity surface emitting lasers in multimode optical fiber links," *Electron. Lett.* **30**, 139–140 (1994).
10. D. Wiedenmann, P. Schnitzer, C. Jung, M. Grabherr, R. Jager, R. Michalzik, and K. J. Ebeling, "Noise characteristics of 850-nm single-mode vertical cavity surface emitting lasers," *Appl. Phys. Lett.* **73**, 717–719 (1998).
11. G. P. Agrawal and G. R. Gray, "Intensity and phase noise in microcavity surface-emitting semiconductor lasers," *Appl. Phys. Lett.* **59**, 399–401 (1991).
12. K.P. Ho, J.D. Walker and J.M. Kahn, "External Optical Feedback Effects on Intensity Noise of Vertical-Cavity Surface-Emitting Lasers," *IEEE J. Quantum Electron.* **5**, 892–895 (1993).
13. L. Raddatz, I.H. White, K.H. Hahn, M.R. Tan and S.Y. Wang, "Noise performance of multimode vertical cavity surface emitting lasers," *Electron. Lett.* **30** 1991–1992 (1994).

14. C.J. Chang-Hasnain, J.P. Harbison, G. Hasnain, A.C. Von Lehmen, L.T. Florez and N.G. Stoffel, "Dynamic, polarization and transverse mode characteristics of VCSELs," *IEEE J. Quantum Electron.* **27**, 1402–1408 (1991).
15. A. Valle, J. Sarma and K.A. Shore, "Spatial hole-burning effects on the dynamics of vertical-cavity surface-emitting laser Diodes," *IEEE J. Quantum Electron.* **31**, 1423–1431 (1995).
16. A. Valle, "Selection and modulation of high-order transverse modes in vertical-cavity surface-emitting lasers," *IEEE J. Quantum Electron.* **34**, 1924–1932 (1998).
17. Y. Satuby and M. Orenstein, "Small-signal modulation of multitransverse modes vertical-cavity surface-emitting semiconductor lasers, *IEEE Photon. Technol. Lett.* **10**, 757–759 (1998).
18. J. Y. Law and G. P. Agrawal, "Effect of spatial hole-burning on gain switching in vertical-cavity surface-emitting lasers," *IEEE J. Quantum Electron.* **33**, 462–468 (1997).
19. J. Y. Law and G. P. Agrawal, "Mode-partition noise in vertical-cavity surface-emitting lasers," *IEEE Photon. Technol. Lett.* **9** 437–439 (1997).
20. J. Y. Law and G. P. Agrawal, "Nonlinear spatio-temporal dynamics due to transverse-mode competition in gain-switched microcavity lasers," *Opt. Commun.* **138**, 95–98 (1997).
21. J. Y. Law and G. P. Agrawal, "Effect of optical feedback on static and dynamic characteristics of vertical-cavity surface-emitting lasers," *IEEE J. Sel. Top. Quantum Electron.* **3**, 353–358 (1997).
22. J. Y. Law, G. H. M. van Tartwijk, and G. P. Agrawal, "Effect of transverse-mode competition on injection dynamics of vertical-cavity surface-emitting lasers," *J. Europ. Opt. Soc. B: Quantum Semiclass. Opt.* **9**, 737–748 (1997).
23. J.Y. Law and G.P. Agrawal, "Feedback-induced Chaos and intensity-noise enhancement in vertical-cavity surface-emitting lasers," *J. Opt. Soc. of Am. B* **15**, 562–569 (1998).
24. G.P. Agrawal and N.K. Dutta, *Semiconductor Lasers*, 2nd ed., Van Nostrand Reinhold, New York, 1993.
25. C.H. Chong and J. Sarma, "Lasing mode selection in vertical-cavity surface-emitting laser diodes," *IEEE Photon. Tech. Lett.* **5**, 761-764 (1993).